

# Shorter $^{146}\text{Sm}$ half-life and revised $^{146}\text{Sm}$ - $^{142}\text{Nd}$ ages of planetary mantle differentiation

N. Kinoshita<sup>1</sup>, M. Paul<sup>2</sup>, Y. Kashiv<sup>3</sup>, P. Collon<sup>3</sup>, C.M. Deibel<sup>4,5</sup>, B. DiGiovine<sup>4</sup>, J.P. Greene<sup>4</sup>,  
D.J. Henderson<sup>4</sup>, C.L. Jiang<sup>4</sup>, S.T. Marley<sup>4</sup>, T. Nakanishi<sup>6</sup>, R.C. Pardo<sup>4</sup>, K.E. Rehm<sup>4</sup>,  
D. Robertson<sup>3</sup>, R. Scott<sup>4</sup>, C. Schmitt<sup>3</sup>, X.D. Tang<sup>3</sup>, R. Vondrasek<sup>4</sup> and A. Yokoyama<sup>6</sup>

<sup>1</sup>*Research Facility Center for Science and Technology, U. of Tsukuba, Japan*

<sup>2</sup>*Racah Institute of Physics, Hebrew University, Jerusalem, Israel 91904*

<sup>3</sup>*Department of Physics, University of Notre Dame, Notre Dame, IN 46556-5670*

<sup>4</sup>*Physics Division, Argonne National Laboratory, Argonne, IL 60439*

<sup>5</sup>*Joint Institute for Nuclear Astrophysics, Michigan State University, East Lansing, MI 48824*

<sup>6</sup>*Faculty of Chemistry, Institute of Science and Engineering, Kanazawa University, Japan*

**The extinct short-lived nuclide  $^{146}\text{Sm}$ , synthesized in stellar events by the  $p$ -process, serves as both an astrophysical and geochemical chronometer through measurements of isotopic anomalies of its  $\alpha$ -decay daughter  $^{142}\text{Nd}$ . Evidence of live  $^{146}\text{Sm}$ , quantitatively established for the early Solar System, constrains the time between  $p$ -process nucleosynthesis and condensation of the first solid materials<sup>1</sup>. Samarium-146 is used also to date silicate mantle differentiation events in a number of planetary bodies, including Earth<sup>2</sup>. We performed a new measurement of the  $^{146}\text{Sm}$  half-life and our result,  $t_{1/2}^{146} = 68 \pm 7$  (1 $\sigma$ ) million year (Ma), is significantly shorter than the value currently used for  $^{146}\text{Sm}$ - $^{142}\text{Nd}$  chronology ( $103 \pm 5$  Ma<sup>3,4</sup>). We show here that the shorter  $^{146}\text{Sm}$  half-life value implies a higher initial Solar System ratio,  $(^{146}\text{Sm}/^{144}\text{Sm})_0 = 0.0094 \pm 0.0005$  (2 $\sigma$ ), than the recently derived value  $0.0085 \pm 0.0007$ <sup>5</sup>, or that used in most studies**

**0.008±0.001<sup>6</sup>. Planetary differentiation processes dated by <sup>146</sup>Sm-<sup>142</sup>Nd converge to a shorter time span, due to the combined effect of the new <sup>146</sup>Sm half-life and (<sup>146</sup>Sm/<sup>144</sup>Sm)<sub>0</sub> values. The revised <sup>142</sup>Nd age of the recently dated Lunar ferroan anorthosite (FAN) 60025<sup>7</sup>, is in agreement with its <sup>147</sup>Sm-<sup>143</sup>Nd age; their weighted average, 196±11 (2σ) Ma after Solar System birth, is consistent with the 208.8±2.4 Ma Pb-Pb age<sup>7</sup> and with the age derived here (170±15 Ma) from an isochron of Lunar rocks<sup>2</sup>.**

The α-decay half-life of the *p*-process <sup>146</sup>Sm nuclide, extinct in the Solar System (SS), was first measured by Dunlavey and Seaborg<sup>8</sup> as ~50 Ma and by Nurmi *et al.* as 74±15 Ma<sup>9</sup>. The current value, 103±5 Ma, is based on the studies of Friedman *et al.*<sup>3</sup> and Meissner *et al.*<sup>4</sup>. Audouze & Schramm<sup>10</sup> proposed to use <sup>146</sup>Sm to study the *p*-process and its chronology in the SS. The suggestion was followed by the first evidence for live <sup>146</sup>Sm: Lugmair & Marti<sup>11</sup> showed a correlation between anomalies in isotopic abundances of <sup>142</sup>Nd, the daughter of <sup>146</sup>Sm, and the Sm content in the Angra Dos Reis meteorite, determining the <sup>146</sup>Sm abundance in the meteorite parent body. The source of extinct radioactivities in the SS, such as <sup>146</sup>Sm, was studied for example by Wasserburg *et al.*<sup>1</sup>, who compared the abundances of short-lived radionuclides derived from meteorites with models of Galactic nucleosynthesis. They concluded that the abundance of <sup>146</sup>Sm (and *r*-process actinides) is compatible with the uniform production (UP) model, expressing secular equilibrium in the interstellar medium (ISM) between production in supernovae and radioactive decay, with a time interval, Δ ≈ 70 Ma, between isolation of the solar nebula from the ISM and the start of SS formation. Neodymium-142 anomalies relative to the chondritic uniform reservoir (CHUR) were observed in a wide range of SS materials: meteorite

parent bodies<sup>6,12,13</sup>, Earth<sup>14-17</sup>, Moon<sup>18-20</sup> and Mars<sup>21-24</sup>. These anomalies, primarily positive, are interpreted as resulting from the slightly higher incompatibility of Nd causing fractionation, while <sup>146</sup>Sm was still live, between a relatively Sm-rich solid phase in the silicate mantle and a relatively Nd-rich liquid phase during partial melting or solidification. It is also hypothesized<sup>2,24</sup> that the Sm/Nd ratio of bulk planetary bodies is 5-10% higher than CHUR, possibly due to fractionation and collisional erosion effects at the planetary accretion stage.

The <sup>146</sup>Sm half-life is an essential ingredient in the cosmochemical interpretation of these studies. By measuring the  $\alpha$ -activity ratio and the atom ratio of <sup>146</sup>Sm to naturally-occurring <sup>147</sup>Sm in activated samples of <sup>147</sup>Sm, we determined the <sup>146</sup>Sm half-life ( $t_{1/2}^{146}$ ) through the equation  $t_{1/2}^{146} = \frac{A_{147}}{A_{146}} \times \frac{N_{146}}{N_{147}} \times t_{1/2}^{147}$ . Here,  $t_{1/2}^{147}$  denotes the <sup>147</sup>Sm alpha-decay half-life ( $107 \pm 9$  billion year (Ga)<sup>25</sup> and  $A_A$ ,  $N_A$  the alpha activity and atom number of <sup>A</sup>Sm in the sample, respectively. The ratio measurement eliminates most systematic uncertainties in determinations of  $\alpha$  activity due to detector efficiency and geometrical acceptance. Three independent <sup>146</sup>Sm source materials were produced by activating <sup>147</sup>Sm isotopically enriched targets via the following nuclear reactions: (i) <sup>147</sup>Sm( $\gamma, n$ )<sup>146</sup>Sm (using 50-MeV electron bremsstrahlung radiation); (ii) 21-MeV proton irradiation through the <sup>147</sup>Sm( $p, 2n\epsilon$ )<sup>146</sup>Sm reaction and (iii) fast-neutron activation <sup>147</sup>Sm( $n, 2n$ )<sup>146</sup>Sm. The Sm targets were then dissolved and Sm purified by liquid chromatography. Spectroscopic alpha sources (20-100  $\mu$ g) from the three activations were prepared and counted during several months using a silicon surface-barrier detector<sup>26</sup> (fig. 1, see Methods section, Supplementary M1 for details). In order to prepare samples for atom ratio measurements, the Sm sources were dissolved and quantitatively diluted with high-purity <sup>nat</sup>Sm in various ratios (see chemical protocol in Supplementary M2), yielding metallic Sm samples of

typically 5-10 mg. Accelerator mass spectrometry (AMS) was used for the determination of the  $^{146}\text{Sm}/^{147}\text{Sm}$  atom ratio because of the need to discriminate isobaric  $^{146}\text{Nd}$  interferences (fig. 1), observed to be critical in our experiment when using thermal-ionization mass spectrometry<sup>27</sup>. The AMS measurements<sup>28</sup> were performed (see Supplementary M3) using the ATLAS facility (Argonne National Laboratory). The measured atom ratio for each activated sample is shown (fig. 2 and Supplementary table S1), divided by the atom ratio expected from its alpha activity, its individual dilution factor and using the currently adopted  $^{146}\text{Sm}$  half-life value of 103 Ma<sup>3,4</sup>. The double ratio, equivalent to the ratio of our measured  $^{146}\text{Sm}$  half-life to that currently adopted, is equal to  $0.66 \pm 0.07$  ( $1\sigma$ ) for samples made from the three independent activation reactions and with different dilution ratios, and corresponds to a  $^{146}\text{Sm}$  half-life value of  $68 \pm 7$  Ma ( $1\sigma$ ). This  $t_{1/2}^{146}$  value has far-reaching implications for SS and planetary chronology.

**1. Initial SS ( $^{146}\text{Sm}/^{144}\text{Sm}$ )<sub>0</sub> ratio and the source of  $^{146}\text{Sm}$  in the SS** Knowledge of the initial ratio ( $^{146}\text{Sm}/^{147}\text{Sm}$ )<sub>0</sub> is key for interpreting the source of SS  $^{146}\text{Sm}$  and for dating differentiation events. While evidence for extinct  $^{146}\text{Sm}$  was found in many meteorites, the majority show chemical and isotopic re-equilibration which potentially altered the initial ratio<sup>6,12,13</sup>. In a recent study, Boyet *et al.*<sup>5</sup> selected a number of meteorites which appear to have remained closed Sm-Nd systems. Using the individual  $^{146}\text{Sm}/^{144}\text{Sm}$  ratios of the meteorites and  $^{147}\text{Sm}$ - $^{143}\text{Nd}$  ages, they re-determined an initial SS value ( $^{146}\text{Sm}/^{147}\text{Sm}$ )<sub>0</sub> =  $0.0085 \pm 0.0007$  ( $2\sigma$ ) (compared to  $0.008 \pm 0.001$  ( $2\sigma$ )<sup>6</sup> used in most studies). As a basis of comparison, we fit the same set of data<sup>5</sup> (fig.3) using our measured  $^{146}\text{Sm}$  half-life and derive a revised initial ratio ( $^{146}\text{Sm}/^{144}\text{Sm}$ )<sub>0</sub> =  $0.0094 \pm 0.0005$  ( $2\sigma$ ). A fit taking into account uncertainties in both age and isotopic ratio leads however to the less precise value  $0.0094^{+0.0018}_{-0.0014}$  ( $2\sigma$ ). It appears that the determination of an experimental  $^{146}\text{Sm}$  decay curve from meteoritic data would require a precision in  $^{146}\text{Sm}$

abundances beyond present capability or more data on relatively young meteorites. The initial ratio  $(^{146}\text{Sm}/^{144}\text{Sm})_0$  results from the decay of  $^{146}\text{Sm}$  ISM abundance during the isolation interval  $\Delta$  and both these quantities depend on the  $^{146}\text{Sm}$  half-life. The initial solar ratio can be expressed<sup>1,29</sup> in terms of the  $(^{146}\text{Sm}/^{144}\text{Sm})_{ISM}$  ISM abundance as

$$\left(\frac{^{146}\text{Sm}}{^{144}\text{Sm}}\right)_0 = \left(\frac{^{146}\text{Sm}}{^{144}\text{Sm}}\right)_{ISM} \exp(-\Delta/\tau) = \frac{P^{146}}{P^{144}} \kappa \frac{\tau}{T} \exp(-\Delta/\tau) \quad (1), \text{ where } P^{146}/P^{144} \text{ denotes the } ^{146,144}\text{Sm}$$

$p$ -process production ratio (taken as  $\sim 1$ ),  $\tau$  the  $^{146}\text{Sm}$  mean life,  $T$  the presolar age of the Galaxy ( $\sim 10$  Ga) and  $\kappa = p(T)/\langle p \rangle$  the ratio of  $p$ -process rate just before SS formation to the average  $p$ -process rate ( $\kappa$  ranging from 1 for the UP (closed box) model<sup>1</sup> to  $\sim 2.7$  for an open-box model<sup>29</sup> with Galactic-disk enrichment in low-metallicity gas). The isolation time  $\Delta$  calculated from eq. (1) with the new half-life and  $(^{146}\text{Sm}/^{144}\text{Sm})_0$  values is reduced by factor of  $\sim 2.5$  -20 from previous estimates to a range of  $\sim 5$  Ma in the closed-box model and  $\sim 100$  Ma in the open-box model.

**2. Earth, Moon and Mars** The  $^{146}\text{Sm}$  decay curve in fig. 3 ( $t_{1/2}^{146} = 68$  Ma,  $(^{146}\text{Sm}/^{147}\text{Sm})_0 = 0.0094$ ) and the two decay curves using  $t_{1/2}^{146} = 103$  Ma (with  $(^{146}\text{Sm}/^{147}\text{Sm})_0 = 0.0085^5$  and  $0.008^6$  used in most studies) intersect in the range of 30-50 Ma. This reduces the age (measured in this work relative to the birth of SS) of events older than  $\sim 50$  Ma, while it has a minor effect on earlier events. The effect is demonstrated in table 1 and results for some key studies are discussed below.

Samarium-146 observations in terrestrial samples can be divided into two groups: (a) most terrestrial rocks display a  $^{142}\text{Nd}/^{144}\text{Nd}$  ratio higher by  $\sim 18$  parts per million (ppm) than CHUR<sup>14</sup> and (b) anomalies in the  $^{142}\text{Nd}/^{144}\text{Nd}$  ratio relative to the terrestrial standard, both positive, in rocks from Greenland and Australia<sup>2,15</sup>, and negative, in rocks from Northern Quebec

and India<sup>2,16,17</sup>. In the case (a), the conclusion that the mantle had to differentiate within 30 Ma in order to account for the observed anomaly<sup>14</sup> is not changed by the new values. On the other hand, ages in (b) change significantly. One case is the differentiation age of the depleted mantle source of Archean rocks<sup>2</sup>. If the array of these rocks is interpreted as an isochron<sup>2</sup>, its age decreases from 170 to 120 Ma. Another example is the isochron which dates the differentiation time of the enriched mantle source of rocks from Quebec<sup>16</sup>. The age here decreases considerably from  $287^{+81}_{-53}$  to  $205^{+54}_{-35}$  Ma.

An array of Lunar rocks<sup>18,20</sup> has been similarly interpreted as an isochron<sup>2</sup> which dates the solidification of the Lunar magma ocean (LMO). The age revised by the <sup>146</sup>Sm half-life is decreased from  $242 \pm 22$  to  $170 \pm 15$  Ma. A recent study by Borg et al.<sup>7</sup> has dated for the first time a Lunar sample, ferroan anorthosite (FAN) 60025, by three methods, Pb-Pb, <sup>147</sup>Sm-<sup>143</sup>Nd and <sup>146</sup>Sm-<sup>142</sup>Nd. Pb-Pb and <sup>147</sup>Sm-<sup>143</sup>Nd gave consistent ages of  $208.8 \pm 2.4$  and  $201 \pm 11$  Ma, respectively, but the <sup>146</sup>Sm-<sup>142</sup>Nd age ( $250^{+38}_{-30}$  Ma) showed a discrepancy. The revised <sup>146</sup>Sm-<sup>142</sup>Nd age of FAN 60025,  $175^{+25}_{-20}$  Ma, becomes consistent with the <sup>147</sup>Sm-<sup>143</sup>Nd age and the weighted average of the two Sm-Nd ages,  $196 \pm 11$  Ma, matches now both the Pb-Pb age of FAN 60025<sup>7</sup> and the Lunar rock isochron<sup>2</sup>.

Foley *et al.*<sup>22</sup> compared nakhlite (Martian) meteorite data with <sup>142</sup>Nd (and <sup>182</sup>W) models. They concluded that the <sup>147</sup>Sm/<sup>144</sup>Nd ratio of the depleted Martian mantle source of these meteorites was  $\sim 0.255$ - $0.266$  (<sup>180</sup>Hf/<sup>183</sup>W =  $\sim 22$ - $43$ ) and the solidification age 8-25 Ma. Reinterpretation with the new values favors the younger end of the age range and suggest that the source was less depleted, with <sup>147</sup>Sm/<sup>144</sup>Nd =  $0.245$  (<sup>180</sup>Hf/<sup>183</sup>W =  $20$ ) (see Supplementary fig. S5). The younger age may be in line with the recent finding that Mars accreted within  $\sim 4$  Ma<sup>30</sup>. Debaille *et al.*<sup>23</sup> and Caro *et al.*<sup>24</sup> inferred a solidification age of 32-40 Ma for the depleted

Martian mantle source of the shergottite meteorites; this range is not affected by the values derived here. A solidification age of ~110 Ma was calculated for the mantle source of enriched shergottites<sup>23</sup>. This age decreases to ~90 Ma with the new decay curve (Supplementary fig. S6). However, it should be noted that an alternative interpretation of the data gave the same ~40 Ma age for these meteorites<sup>24</sup>.

**Table 1: The effect of the shorter  $^{146}\text{Sm}$  half-life on estimated time of differentiation events.**

Planetary body	Sample / Mantle differentiation event	Reference	Time after start of SS formation (Ma)	
			From ref. in col. 3 <sup>a</sup>	Revised in present work <sup>b</sup>
Earth	Terrestrial rocks 20 ppm above CHUR / depleted–enriched reservoirs	14	$\leq 30$	No change
	Archean array / depleted source	2	170 <sup>c</sup>	120 <sup>d</sup>
	Nuvvuagittuq greenstone belt, Northern Quebec, Canada / enriched source <sup>e</sup>	16	287 <sup>+81</sup> <sub>-53</sub>	205 <sup>+54</sup> <sub>-35</sub> <sup>f</sup>
Moon	Lunar array / LMO solidification <sup>g</sup>	2	242 ± 22	170 ± 15 <sup>h</sup>
	FAN 60025 / LMO solidification <sup>g,i</sup>	7	250 <sup>+38</sup> <sub>-30</sub>	175 <sup>+25</sup> <sub>-20</sub> <sup>j</sup>
Mars	Nakhlites / Solidification of depleted source	22	8 – 25 <sup>k</sup>	Favors young age <sup>l</sup>
	Enriched shergottites / Solidification of source	23	~110	~90 <sup>m</sup>

<sup>a</sup> Derived in the original studies (col. 3) using  $t_{1/2}^{146} = 103$  Ma,  $(^{146}\text{Sm}/^{147}\text{Sm})_0 = 0.008$ ,  $t_0 = 4,567$

Ma (see text).

<sup>b</sup> Derived using present values  $t_{1/2}^{146} = 68$  Ma,  $(^{146}\text{Sm}/^{147}\text{Sm})_0 = 0.0094$ , and  $t_0 = 4,568$  Ma (see text).

<sup>c</sup> Using  $(^{146}\text{Sm}/^{147}\text{Sm})_0 = 0.0085$ .

<sup>d</sup> Reinterpretation of fig. 3 of Caro<sup>2</sup>.

<sup>e</sup> Measured in > 3,800 Ma faux-amphibolite and gabbro.

<sup>f</sup> Reinterpretation of fig. 3 of O'Neil *et al.*<sup>16</sup>.



<sup>g</sup> LMO = Lunar magma ocean.

<sup>h</sup> Reinterpretation of fig. 8 of Caro<sup>2</sup>.

<sup>i</sup> FAN = ferroan anorthosite.

<sup>j</sup> Reinterpretation of fig. 2b of Borg *et al.*<sup>7</sup>.

<sup>k</sup> Calculated  $^{147}\text{Sm}/^{144}\text{Nd} \sim 0.255\text{-}0.266$  ( $^{180}\text{Hf}/^{183}\text{W} = \sim 22\text{-}43$ ) for the Martian mantle source.

<sup>l</sup> Calculated  $^{147}\text{Sm}/^{144}\text{Nd} \sim 0.245$  ( $^{180}\text{Hf}/^{183}\text{W} \sim 20$ ) for the Martian mantle source. See SI, fig. S5.

<sup>m</sup> See SI, fig. S6.

## References

1. Wasserburg, G. J., Busso, M., Gallino, R. & Nollett, K. M., Short-lived nuclei in the early Solar System: Possible AGB sources. *Nucl. Phys. A* **777**, 5–69 (2006)
2. Caro, G., Early silicate earth differentiation. *Annu. Rev. Earth Planet. Sci.*, **39**, 31-58 (2011)
3. Friedman, A. M. et al., Alpha decay half lives of  $^{148}\text{Gd}$ ,  $^{150}\text{Gd}$  and  $^{146}\text{Sm}$ . *Radiochim. Acta* **5**, 192-194 (1966)
4. Meissner, F., Schmidt-Ott, W.-D. & Ziegeler, L., Half-life and  $\alpha$ -energy of  $^{146}\text{Sm}$ . *Z. Phys. A* **327**, 171-174 (1987)
5. Boyet, M., Carlson, R. W. & Horan, M., Old Sm–Nd ages for cumulate eucrites and redetermination of the solar system initial  $^{146}\text{Sm}/^{144}\text{Sm}$  ratio. *Earth Planet. Sci. Lett.* **291**, 172–181 (2010)
6. Nyquist, L. E., Bansal, B., Wiesmann, H. & Shih, C.-Y. Neodymium, strontium and chromium isotopic studies of the LEW86010 and Angra dos Reis meteorites and the chronology of the angrite parent body. *Meteoritics* **29**, 872–885 (1994)
7. Borg, L. E., Connelly, J. N., Boyet, M. & Carlson, R. W. Chronological evidence that the Moon is either young or did not have a global magma ocean. *Nature* **477**, 70-72 (2011)
8. Dunlavey, D. C. & Seaborg, G. T. 1953, Alpha activity of  $^{146}\text{Sm}$  as Detected with Nuclear Emulsions. *Phys. Rev.* **92** 206 (1953)
9. Nurmi M., Graeffe, G, Valli, K. & Aaltonen, J, Alpha activity of Sm-146. *Ann. Acad. Scient. Fenn. A.VI.* **148**, 1-8 (1964)
10. Audouze, J. & Schramm, D. N.,  $^{146}\text{Sm}$ : A chronometer for p-process nucleosynthesis. *Nature* **237**, 447-449 (1972)

11. Lugmair, G. W. & Marti, K., Sm-Nd-Pu time pieces in the Angra dos Reis meteorite. *Earth Planet. Sci. Lett.* **35**, 273-284 (1977)
12. Prinzhofer, A., Papanastassiou, D. A. & Wasserburg, G. J., Samarium-neodymium evolution of meteorites. *Geochim. Cosmochim. Acta* **56**, 797-815 (1992)
13. Stewart, B. W., Papanastassiou, D. A. & Wasserburg, G. J., Sm-Nd chronology and petrogenesis of mesosiderites. *Geochim. Cosmochim. Acta* **58**, 3487–3509 (1994)
14. Boyet, M. & Carlson, R. W.,  $^{142}\text{Nd}$  evidence for early ( $> 4.53$  Ga) global differentiation of the silicate Earth, *Science* **309**, 576–581 (2005)
15. Bennett, V. C., Brandon, A. D. & Nutman, A. P., Coupled  $^{142}\text{Nd}$ - $^{143}\text{Nd}$  isotopic evidence for Hadean mantle dynamics. *Science* **318**, 1907–1910 (2007)
16. O’Neil, J., Carlson, R. W., Francis, D. & Stevenson, R. K., Neodymium-142 evidence for Hadean mafic crust, *Science* **321**, 1828–1831 (2008)
17. Upadhyay, D., Scherer, E. E. & Mezger, K.,  $^{142}\text{Nd}$  evidence for an enriched Hadean reservoir in cratonic roots. *Nature* **459**, 1118-1121 (2009)
18. Nyquist, L. E. et al.,  $^{146}\text{Sm}$ – $^{142}\text{Nd}$  formation interval for the lunar mantle. *Geochim. Cosmochim. Acta* **59**, 2817–2837 (1995)
19. Rankenburg, K., Brandon, A. D. & Neal, C. R., Neodymium isotope evidence for a chondritic composition of the Moon. *Science* **312**, 1369–1372 (2006)
20. Boyet, M. & Carlson, R. W., A highly depleted moon or a non-magma ocean origin for the lunar crust? *Earth Planet. Sci. Lett.* **262**, 505–516 (2007)
21. Harper, C. L. Jr, Nyquist, L. E., Bansal, B., Wiesmann, H. & Shih, C.-Y., Rapid accretion and early differentiation of Mars indicated by  $^{142}\text{Nd}/^{144}\text{Nd}$  in SNC meteorites. *Science* **267**, 213–217 (1995)

22. Foley, C. N., Wadhwa, M., Borg, L. E., Janney, P.E., Hines, R. & Grove, T. L., The early differentiation history of Mars from  $^{182}\text{W}$ - $^{142}\text{Nd}$  isotope systematics in the SNC meteorites. *Geochim. Cosmochim. Acta* **69**, 4557–4571 (2005)
23. Debaille, V., Brandon, A. D., Yin, Q. Z. & Jacobsen, B., Coupled  $^{142}\text{Nd}$ – $^{143}\text{Nd}$  evidence for a protracted magma ocean in Mars. *Nature* **450**, 525–528 (2007)
24. Caro, G., Bourdon, B., Halliday, A. N. & Quitté, G., Super-chondritic Sm/Nd ratios in Mars, the Earth and the Moon. *Nature* **452**, 336–339 (2008)
25. Kossert, K., Joerg, G., Naehle, O., Lierse, C. & v. Gostomski, C. L.. High-precision measurement of the half-life of  $^{147}\text{Sm}$ . *Appl. Rad. Isot.* **67**, 1702-1706 (2009)
26. Kinoshita, N. et al., Technological development for half-life measurement of  $^{146}\text{Sm}$  nuclide. *J. Nucl. Radiochem. Sci.* **8**, 109-112 (2007)
27. Tazoe, H., Obata. H., Amakawa H., Nozaki Y. and Gamo T., Precise determination of the cerium isotopic compositions of surface seawater in the Northwest Pacific Ocean and Tokyo Bay. *Mar. Chem.* **103**, 1-14 (2007)
28. Kinoshita, N. et al., Ultra-sensitive detection of  $p$ -process nuclide  $^{146}\text{Sm}$  produced by  $(\gamma, n)$ ,  $(p, pn\epsilon)$  and  $(n, 2n)$  reactions. *J. Phys. G: Nucl. Part. Phys.* **35**, 014033 (2008)
29. Dauphas N., Rauscher T., Marty B. and Reisberg L., Short-lived  $p$ -nuclides in the early solar system and implications on the nucleosynthetic role of X-ray binaries, *Nucl. Phys.* A719, 287c-295c (2003)
30. Dauphas, N. & Pourmand, A. Hf–W–Th evidence for rapid growth of Mars and its status as a planetary embryo. *Nature* **473**, 489–493 (2011)

## Figure legends

**Figure 1:** (left) Alpha spectra from activated  $^{147}\text{Sm}$  via  $(\gamma,n)$ ,  $(n,2n)$  and  $(p,2n\epsilon)$ , determining the  $^{146}\text{Sm}/^{147}\text{Sm}$  activity ratio; (right) Identification spectra measured for a  $(n,2n)$  activated sample (upper right) and non-activated  $^{\text{nat}}\text{Sm}$  (lower right). The spectrum displays energy loss vs. position signals from a detector along the focal plane of a gas-filled magnetic spectrograph. The device separates in position (magnetic rigidity)  $^{146}\text{Sm}^{22+}$  ions from  $^{146}\text{Nd}^{22+}$  isobaric ions (originating from chemical impurities in the sample or in ion source structural material), owing to their different average ionic charge state in the gas (Supplementary M3). The observed  $^{126}\text{Xe}^{19+}$  group is transmitted by the accelerator due to its charge-to-mass ratio quasi-degenerate with that of  $^{146}\text{Sm}^{22+}$  and originates from residual gas in the ion source. In order to determine the  $^{146}\text{Sm}/^{147}\text{Sm}$  ratios (Supplementary table S1), the count rate in the  $^{146}\text{Sm}$  group was normalized to  $^{147}\text{Sm}$ , alternately transported through the accelerator: the  $^{147}\text{Sm}^{22+}$  or  $^{147}\text{Sm}^{23+}$  charge currents (with appropriate correction for the charge state fraction) were measured in an electron-suppressed Faraday Cup before the spectrograph or the  $^{147}\text{Sm}^{22+}$  ion count rate was measured in the same detector as  $^{146}\text{Sm}$  after quantitative beam attenuation; see Supplementary M3 for details. The blank spectrum shown for the  $^{\text{nat}}\text{Sm}$  sample (lower right) corresponds to a ratio  $^{146}\text{Sm}/^{147}\text{Sm} < 10^{-11}$ .

**Figure 2:** Double ratios of the  $^{146}\text{Sm}/^{147}\text{Sm}$  atom ratio measured by AMS to that expected in the same sample from its  $^{146}\text{Sm}/^{147}\text{Sm}$   $\alpha$  activity ratio using the  $^{146}\text{Sm}$  currently adopted half-life (103 Ma). The notations G-x, N-x, P-x on the horizontal axis denote various samples independently prepared from the bremsstrahlung, neutron and proton irradiations, respectively (see Supplementary table S1). The double ratio is equivalent to the ratio of our  $^{146}\text{Sm}$  measured half-life to the adopted value (right vertical axis). The dashed line would correspond to a ratio of

1. The (unweighted) mean and standard deviation ( $0.66 \pm 0.7$ ) of the ratios correspond to a  $^{146}\text{Sm}$  half-life of  $68 \pm 7$  Ma (see text). The measured  $^{146}\text{Sm}/^{147}\text{Sm}$  atom ratios were obtained by dividing the  $^{146}\text{Sm}^{22+}$  count rate with the  $^{147}\text{Sm}^{22+}$  charge current in an electron-suppressed Faraday cup at the spectrograph entrance. The solid squares (for samples N-7 and N-8) correspond to measurements using a (quantitatively attenuated) count rate of  $^{147}\text{Sm}^{22+}$  ions in the same detector as for  $^{146}\text{Sm}^{22+}$  ions, avoiding possible systematic uncertainties in the charge current measurement and transmission efficiency between Faraday cup and detector (Supplementary M3).

**Figure 3:** Derivation of the initial Solar System ( $^{146}\text{Sm}/^{144}\text{Sm}$ )<sub>0</sub> ratio from meteorite data using the  $^{146}\text{Sm}$  half-life value measured in this work. To allow direct comparison, the set selected by Boyet et al.<sup>5</sup> as closed Sm-Nd systems is used here: 4 eucrites (Moore County, EET87520, Caldera, Binda), one mesosiderite (Mt. Padbury) and one angrite (LEW 86010). For the latter, a weighted average of the age and isotopic ratio of two measurements<sup>5</sup> was used here. Two additional eucrites (Y980318/433), with lower isotopic ratios, are shown but not included in the calculation<sup>5</sup>. The new fitted decay curve (solid line,  $t_{1/2} = 68$  Ma,  $r_0 = (^{146}\text{Sm}/^{144}\text{Sm})_0 = 0.0094$ ), the curve from Boyet and Carlson<sup>5</sup> (dashed,  $t_{1/2} = 103$  Ma,  $r_0 = 0.0085$ ) and that used in most studies<sup>6</sup> (dotted,  $t_{1/2} = 103$  Ma,  $r_0 = 0.008$ ) are shown. The age of the SS is taken as 4568 Ma.

**Supplementary Information:** Supplementary information, enclosed with this manuscript, includes a Methods section ( $^{147}\text{Sm}$  activations, protocol of chemical procedure, AMS measurement at the ATLAS facility); table of measured alpha-activity and atom ratios; six additional figures and legends.

**Acknowledgements:** We gratefully acknowledge discussions with R.W. Carlson and K. M. Nollett. This work is supported in part by Grant-in-Aid for Scientific Research Program of Japan Society for the Promotion of Science (20740161). This work is supported by the U.S. Department of Energy, Office of Nuclear Physics, under contract No. DE-AC02-06CH11357. and by the NSF JINA Grant No. PHY0822648.

**Author Contributions :** N.K., T.N., M.P. and A.Y. conceived the experiment. N.K. performed the activations, alpha-activity measurements and sample preparations. M.P. coordinated the experiment. Y.K. and M.P. wrote the paper. C.M.D., B.D.G., J.G., D.J. H., C.L.J., S.T.M., R.C.P., K.E.R., R.S. and R.V. set up and ran the AMS experimental setup. P.C., C.M.D., Y.K., N.K., S.T.M., M.P., R.C.P, K.E.R., D.R., C.S. and X.D.T. took the AMS measurements.

**Author Information :** The authors declare no competing financial interests. Correspondence and requests for materials should be addressed to M.P. ([paul@vms.huji.ac.il](mailto:paul@vms.huji.ac.il)).

Figure 1

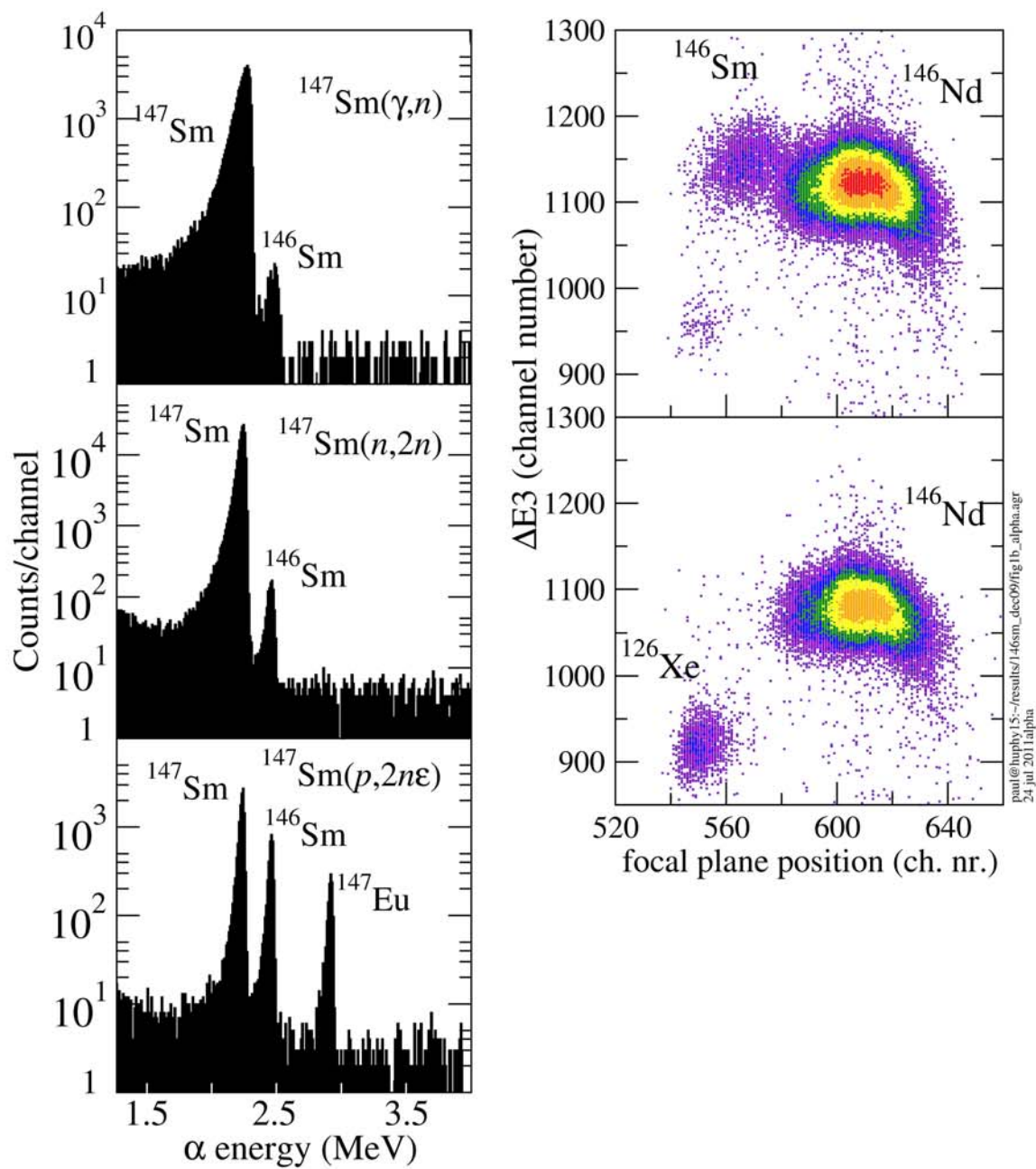
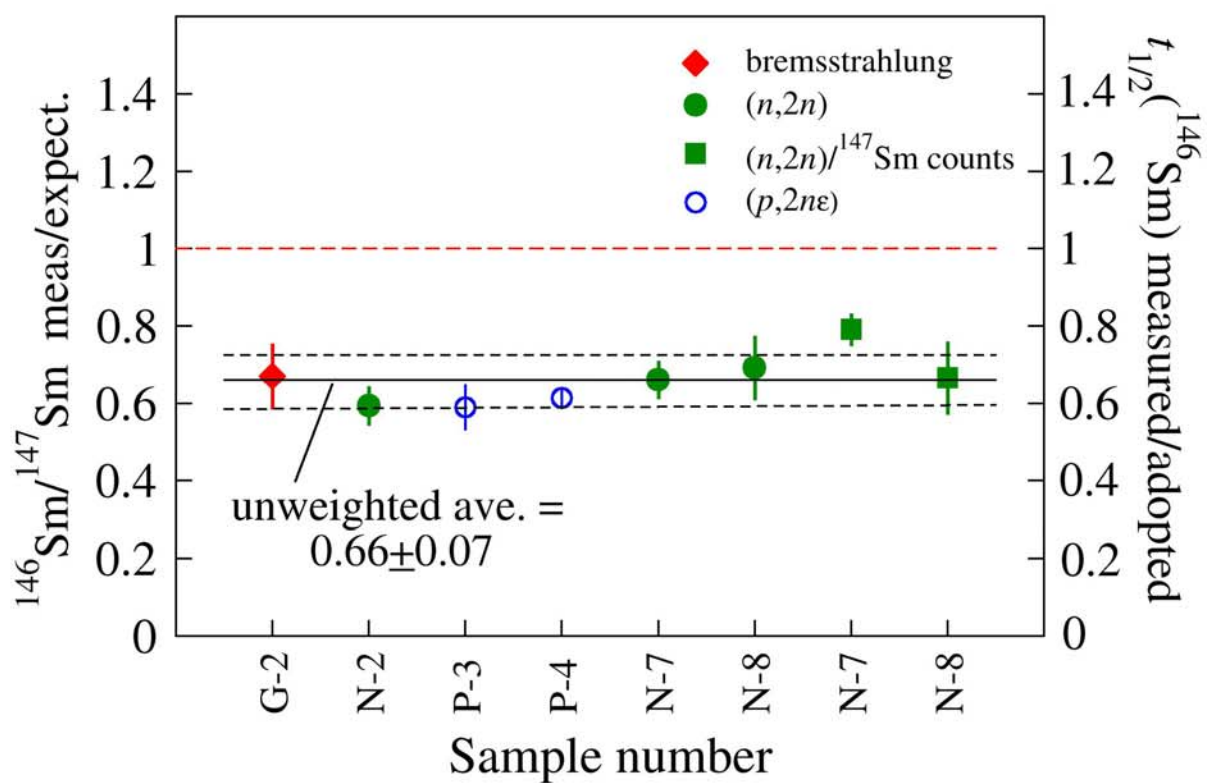


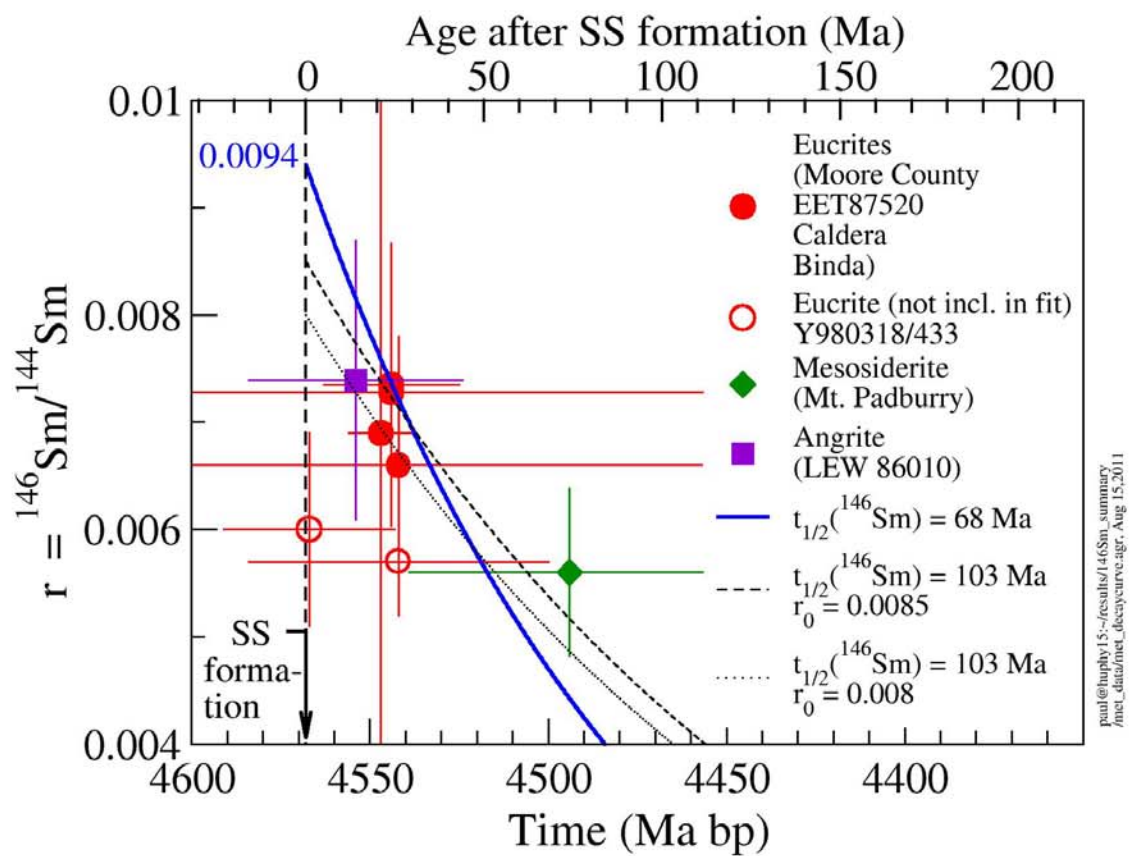


Figure 2



21 Feb '11 paul@huphy15:~/results/146Sm\_summary/  
/huphy21/figs/fig2\_ave\_ratios.agr

Figure 3



### **Supplementary information:**

The Supplementary information contains the following sections:

#### **1. Methods:**

- M1: Activation of  $^{147}\text{Sm}$ , sample preparation for alpha-activity and AMS measurements
- M2 : Chemical protocol
- M3 : Detection of  $^{146}\text{Sm}$  by accelerator mass spectrometry at the ATLAS facility

#### **2. Table S1:**

Alpha-activity and atom ratios of  $^{146}\text{Sm}$  and  $^{147}\text{Sm}$  in the activated samples measured in this experiment.

#### **3. Figures S1 to S6:**

##### **Figure legends:**

**Figure S1:** Charge state distribution measured after the first analysis magnet following the ECR ion source for a metallic sample of enriched  $^{152}\text{Sm}$ . The magnet current on the horizontal axis determines the magnetic field of the injection mass spectrometer. The analyzed beam current (vertical axis) was measured in a Faraday cup at the object position of the injection spectrometer. Charge state 22+, 23+ were used in the experiment.

**Figure S2:** Isotopic ratio  $^{152}\text{Sm}/^{147}\text{Sm}$  measured during our experiment using a similar accelerator scaling procedure as for the ratio  $^{146}\text{Sm}/^{147}\text{Sm}$ . The mean value is  $1.8 \pm 0.2$ , consistent with the natural ratio.

**Figure S3:** Individual (repeat) determinations of the double ratios of the  $^{146}\text{Sm}/^{147}\text{Sm}$  atom ratio measured by AMS in individual repeat measurements of various samples to that expected in the same sample from its  $^{146}\text{Sm}/^{147}\text{Sm}$   $\alpha$  activity ratio using the  $^{146,147}\text{Sm}$  currently adopted half-lives.

The double ratio is equivalent to the ratio of the presently measured  $^{146}\text{Sm}$  half-life to that adopted in the literature. The atom ratios are normalized to the charge current of  $^{147}\text{Sm}^{22+}$  measured in an electron-suppressed Faraday Cup in front of the gas-filled magnetic spectrograph.

**Figure S4a:**  $^{146}\text{Sm}/^{147}\text{Sm}$  atom ratios measured in Exp.3 (see fig. S3) relative to  $^{147}\text{Sm}^{22+}$  charge current.

**Figure S4b:**  $^{146}\text{Sm}/^{147}\text{Sm}$  atom ratios measured relative to  $^{147}\text{Sm}^{22+}$  counts after quantitative attenuation of  $10^5$ . The measured ratios are consistent with those measured relative to  $^{147}\text{Sm}^{22+}$  charge (fig. S4a).

**Figure S5:** Reinterpretation of the differentiation age and  $^{147}\text{Sm}/^{144}\text{Nd}$  ratio of the depleted Martian mantle source of the nakhlite meteorites measured by Foley *et al.*<sup>22</sup>, using the values derived here  $t_{1/2}^{146} = 68 \pm 7$ ,  $(^{146}\text{Sm}/^{144}\text{Sm})_0 = 0.0094 \pm 0.0005$ ; compare with their fig. 5. The axes represent  $\varepsilon^{142}\text{Nd}$  vs.  $\varepsilon^{182}\text{W}$  (see  $\varepsilon$  definitions below). Black curves are models calculated by Foley *et al.*<sup>22</sup>: upper curve is a majorite-bearing deep mantle (MDM) source,  $^{147}\text{Sm}/^{144}\text{Nd} \sim 0.303$  and  $^{180}\text{Hf}/^{183}\text{W} \sim 12$ ; lower curve is garnet-bearing shallow mantle (GSM) source,  $^{147}\text{Sm}/^{144}\text{Nd} \sim 0.266$  and  $^{180}\text{Hf}/^{183}\text{W} \sim 43$ . Blue curves are depleted mantle models calculated by Kleine *et al.*<sup>31</sup>: upper curve is a source with  $^{147}\text{Sm}/^{144}\text{Nd} = 0.281$  and  $^{180}\text{Hf}/^{183}\text{W} = 27$ , middle curve is a source with  $^{147}\text{Sm}/^{144}\text{Nd} = 0.255$  and  $^{180}\text{Hf}/^{183}\text{W} = 22$ , lower curve is a source with  $^{147}\text{Sm}/^{144}\text{Nd} = 0.231$  and  $^{180}\text{Hf}/^{183}\text{W} = 18$ . Open circles on curves indicate ages in Ma after start of SS formation. Ages labeled with Ma refer to the open circles on the black curves. Labeled dashed black lines connect same age points on blue curves. The mean data point is best matched by a composition  $^{147}\text{Sm}/^{144}\text{Nd} = 0.245$  and  $^{180}\text{Hf}/^{183}\text{W} = 20$  (green curve). This composition is less

depleted than that inferred in Foley *et al.*<sup>22</sup>, where the data were best explained by  $^{147}\text{Sm}/^{144}\text{Nd} = 0.255$ - $0.266$  and  $^{180}\text{Hf}/^{183}\text{W} = 22$ - $43$ . In addition, the reinterpretation of the data favors the younger part of the 8-25 Ma age range inferred in the original paper.

All models were calculated with eqs. 5-6 of Foley *et al.*<sup>22</sup> and the parameters therein, with the exception of the parameters derived here,  $t_{1/2}^{146}$  and  $(^{146}\text{Sm}/^{144}\text{Sm})_0$ . The deviation of the Nd isotopic composition from CHUR at a given  $t$  (bp), in  $\epsilon$  units of  $10^{-4}$ , is defined as,

$$\epsilon^i\text{Nd}(t) = \left( \frac{\left( ^i\text{Nd}/^{144}\text{Nd} \right)_t^{\text{DM}}}{\left( ^i\text{Nd}/^{144}\text{Nd} \right)_t^{\text{CHUR}}} - 1 \right) \times 10^4 \quad \text{where } i = 142, 143, \text{ and DM stands for depleted mantle.}$$

Similarly,  $\epsilon^{182}\text{W}$  is defined as:  $\epsilon^{182}\text{W}(t) = \left( \frac{\left( ^{182}\text{W}/^{183}\text{W} \right)_t^{\text{DM}}}{\left( ^{182}\text{W}/^{183}\text{W} \right)_t^{\text{standard}}} - 1 \right) \times 10^4$

**Figure S6:** Reinterpretation of the differentiation age of the Martian mantle source of the shergottite meteorites measured by Debaille *et al.*<sup>23</sup> (solid squares), using the values derived here  $t_{1/2}^{146} = 68 \pm 7$  Ma and  $(^{146}\text{Sm}/^{144}\text{Sm})_0 = 0.0094 \pm 0.0005$ ; compare with their fig. 2. The axis represent  $\epsilon^{142}\text{Nd}$  (rel. to the terrestrial standard) vs.  $\epsilon^{143}\text{Nd}$  at  $t = 150$  Ma before present (bp). Green squares – depleted shergottites, yellow square – intermediate shergottite, red squares – enriched shergottites. Alternating black and blue diagonal dashed lines are loci of the labeled equal mantle depletion ages (Ma bp). Alternating black and blue curved solid lines are loci of the labeled equal  $^{147}\text{Sm}/^{144}\text{Nd}$  ratios. Solid black diagonal line is a mixing line between the different shergottite groups. Differentiation age of the enriched shergottite source is determined by the isochron which passes through the intersection of the mixing line and the  $^{147}\text{Sm}/^{144}\text{Nd} = 0.159$  line<sup>23</sup>. In our figure, it is the (dashed green) 4,476 Ma isochron line that corresponds to ~90 Ma after the start of SS formation (taken as 4,568 Ma bp). Note that Caro *et al.*<sup>24</sup> interpreted the mixing line as an isochron. In this case, all shergottite groups came from one depleted Martian mantle source with a differentiation age of 32-40 Ma. Lines (except mixing) were calculated

with eqs. 1-2. of Debaille *et al.*<sup>23</sup> and their parameters, with the exception of the parameters derived here,  $t_{1/2}^{146}$  and  $(^{146}\text{Sm}/^{144}\text{Sm})_0$ . The definition of  $\epsilon^{\text{iNd}}$  is given in caption of figure S5.

## Methods M1: Activation of $^{147}\text{Sm}$ , sample preparation for alpha-activity and AMS measurements

Three independent  $^{146}\text{Sm}$  source materials were produced for the experiments by activating isotopically enriched targets of  $^{147}\text{Sm}$  via the following nuclear reactions: (i)

$^{147}\text{Sm}(\gamma, n)^{146}\text{Sm}$  (using bremsstrahlung radiation with an end-point energy of 50 MeV from the Electron Linear Accelerator at Tohoku University, Japan); (ii)  $^{147}\text{Sm}(p, 2n)^{146}\text{Sm}$  (using 21 MeV protons from the AVF cyclotron at Osaka University, Japan) and (iii)  $^{147}\text{Sm}(n, 2n)^{146}\text{Sm}$  (using fast neutrons from the Japan Material Testing Reactor, Oarai,

Japan). Following the activations, the Sm targets were dissolved and Sm was purified (see protocol of chemical procedure below). In the case of the proton-induced activation, Eu was separated from the Sm target and  $^{146}\text{Eu}$  let to decay to  $^{146}\text{Sm}$  for about three months.

$^{146}\text{Sm}$  decay products and residual Sm were then chemically separated and purified.

Spectroscopic alpha sources (20-100  $\mu\text{g}$ ) from the three activations were prepared by precipitation onto teflon micropore filters (4.9  $\text{cm}^2$  filtering area).  $\alpha$  activities (fig. 1, see table S1) were measured during several months using a silicon surface-barrier detector of 450  $\text{mm}^2$  active area and  $\sim 20\%$  efficiency<sup>26</sup>.

In order to prepare samples for atom ratio measurements, the Sm sources were dissolved, quantitatively diluted with high-purity  $^{\text{nat}}\text{Sm}$  in various ratios (table S1), in order to have samples of typically 10 mg having an effective natural Sm isotopic composition. The solutions were purified of Nd impurities by repeated liquid-chromatography steps using a lanthanide-specific resin (Ln resin, manufactured by Eichrom Ltd.); see protocol below. The samples were eventually reduced to high-purity Sm metal, observed to have higher ionization yields in the Electron Cyclotron Resonance (ECR) ion source (see below). This was performed by the following steps for each individual sample: (i) Sm hydroxide was

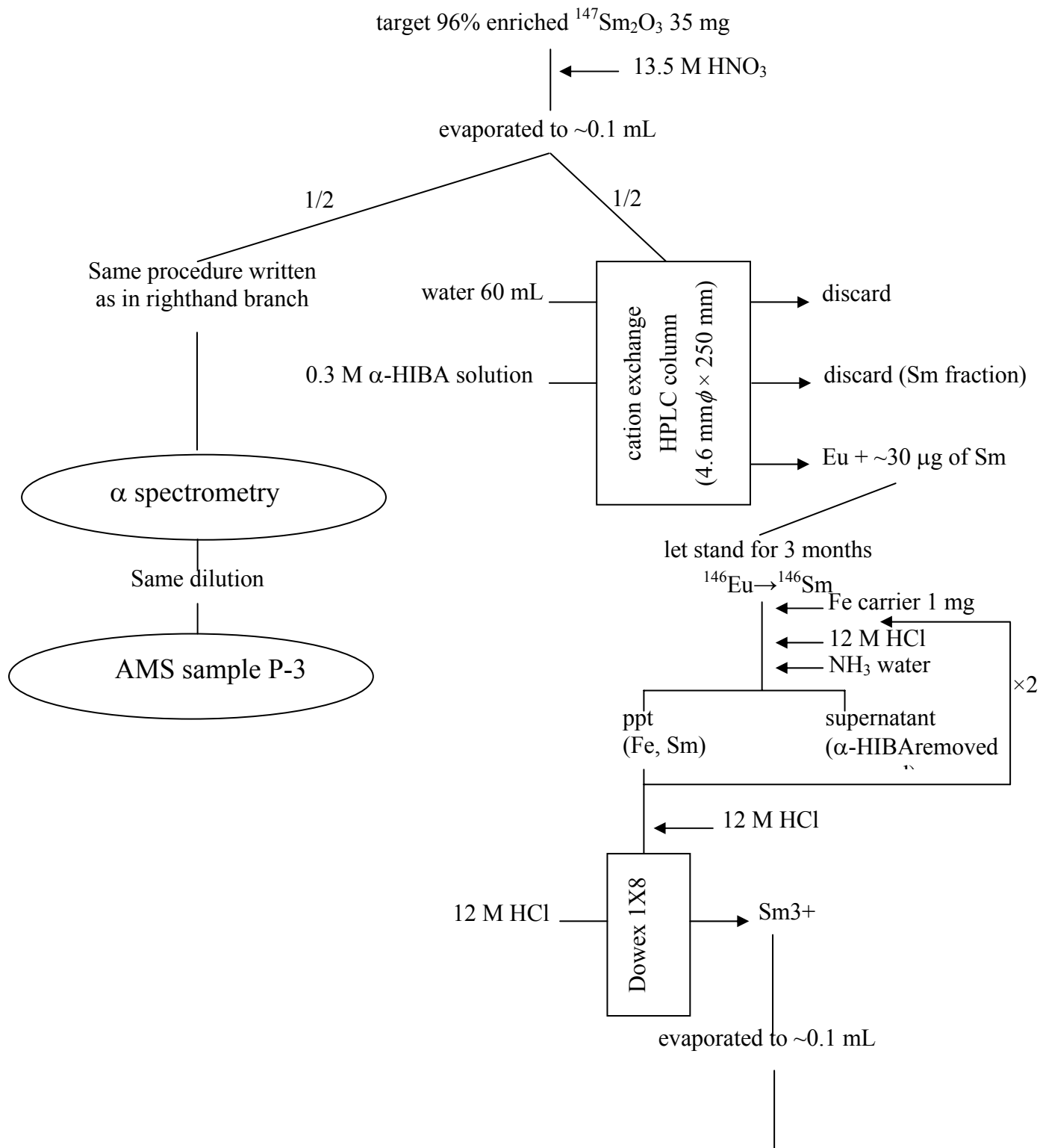
precipitated with an ammonia solution and evaporated to dryness; (ii) ignition to oxide in a quartz crucible at 600°C; (iii) the oxide was thoroughly mixed with freshly filed Zr powder and pressed to 3mm diameter pellets; (iv) the pellets were introduced in a tightly fitting cylindrical tube made of 4 mil thick Ta having a 1 mm diameter orifice; (v) the sealed tube was then placed in a high-vacuum ( $10^{-7}$  Torr) evaporator and resistively heated to  $\sim 1300^{\circ}\text{C}$ ; (vi) reduced and evaporated metallic Sm was collected by distillation on a water-cooled Cu collector placed just above the 1-mm orifice. The Sm sample was eventually pressed in a holder made of high-purity Al to be used as sputter cathode in the ECR ion source.

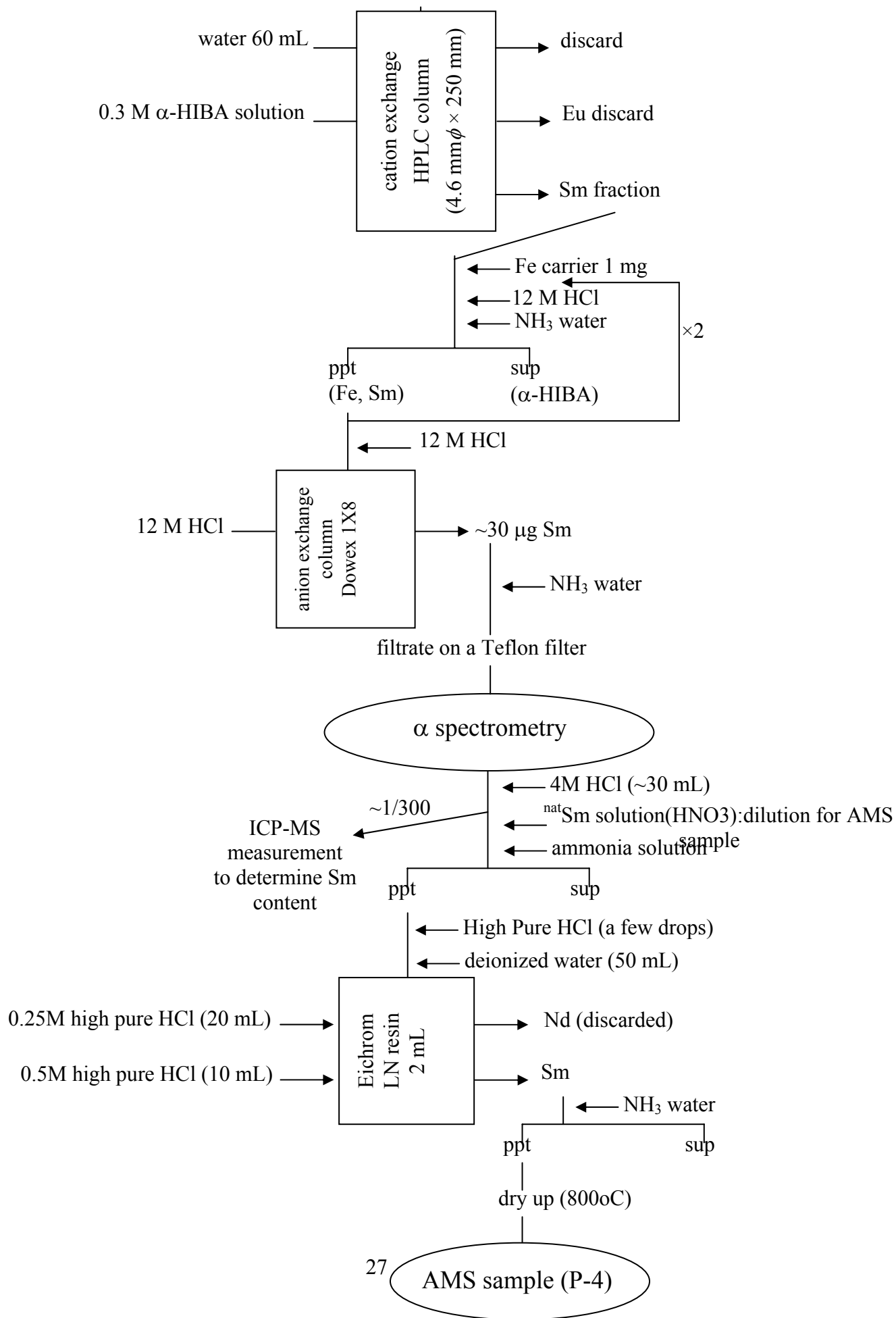


## **M2: Protocol and chemical procedures**

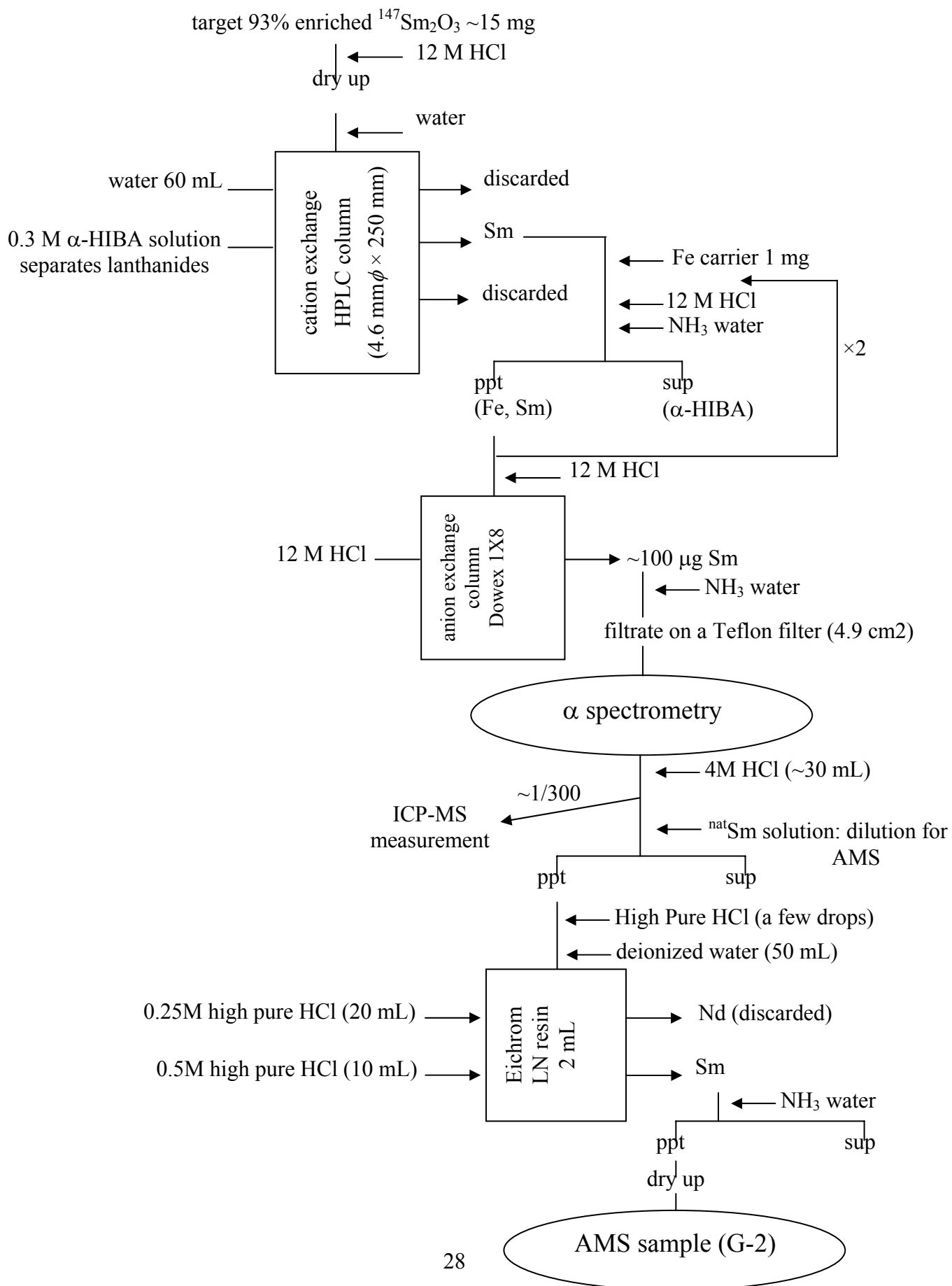
Protocols and chemical procedures used to prepare the activated samples for alpha-activity and atom ratio measurements are shown below as flow charts.

## Chemistry of (p,2n $\epsilon$ ) sample Px



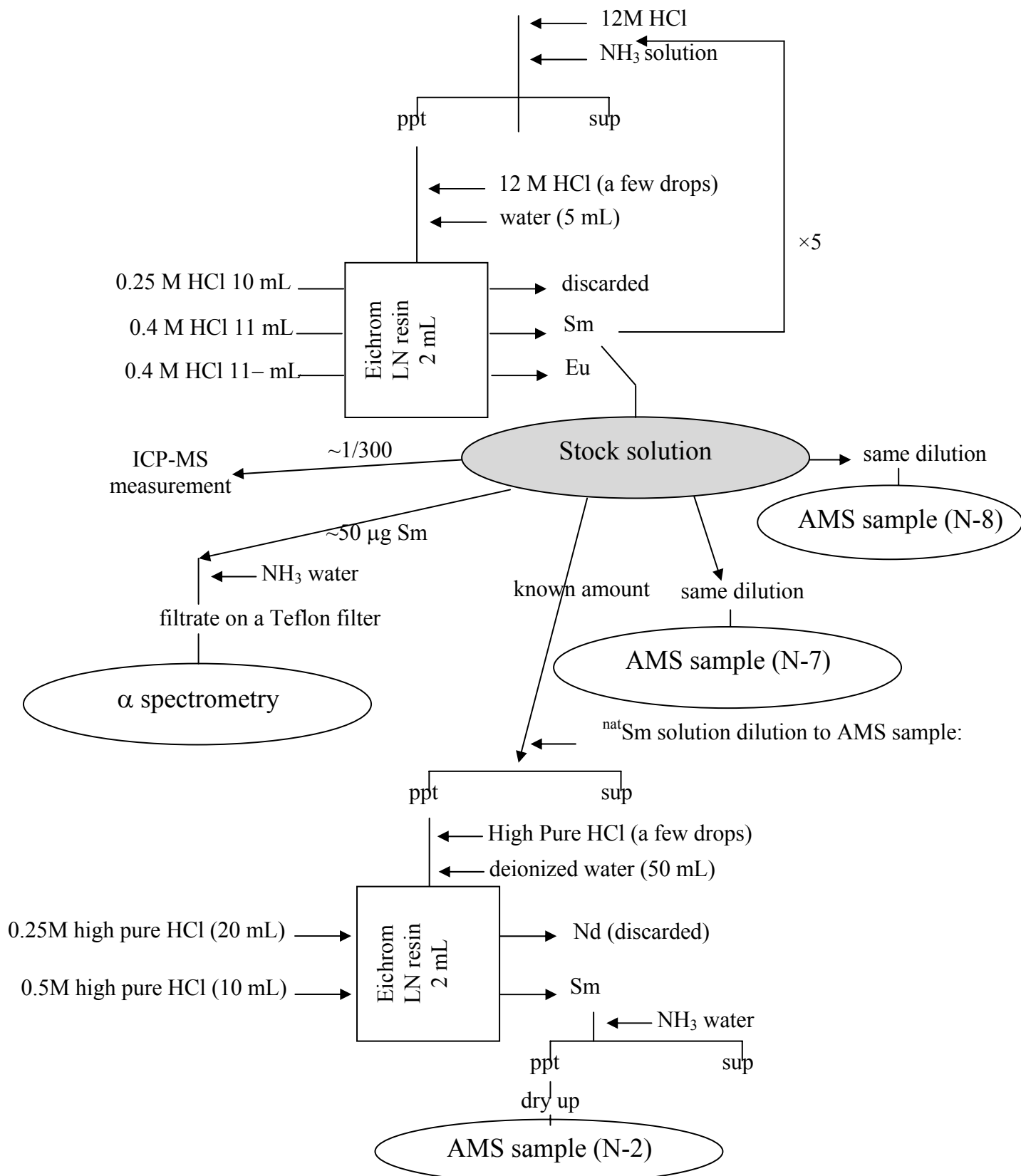


## Chemistry of ( $\gamma,n$ ) sample Gx



## Chemistry of (n,2n) sample Nx

target 96% enriched  $^{147}\text{Sm}_2\text{O}_3$  12.0 mg



### **M3: Detection of $^{146}\text{Sm}$ by accelerator mass spectrometry at the ATLAS facility**

Accelerator mass spectrometry (AMS) was used for the determination of  $^{146}\text{Sm}/^{147}\text{Sm}$  because of the need to discriminate isobaric  $^{146}\text{Nd}$  originating in residual impurities and in structural materials of the ion source. The AMS  $^{146}\text{Sm}/^{147}\text{Sm}$  measurements were made with the Electron Cyclotron Resonance Ion Source (ECRIS)-ATLAS accelerator facility at Argonne National Laboratory.

Highly-charged positive ions are produced in the plasma chamber of the ECRIS<sup>32</sup> by ion sputtering of the Sm metallic sample. In order to reduce background of parasitic ions, the chamber walls were lined with a closely fit cylinder made of quartz transparent to the microwave radiation ( $\sim 100\text{W}$  at  $14\text{ GHz}$ ) which ignites and maintains the plasma.  $^{146}\text{Sm}^{22+}$  and  $^{147}\text{Sm}^{22+}$  ions, alternatively selected by magnetic separation, are bunched and accelerated to a final energy of  $6\text{ MeV}/u$  in the superconducting linear accelerator. Acceleration of neighboring isotopes such as  $^{146}\text{Sm}$  and  $^{147}\text{Sm}$ , both in  $22+$  charge state, requires adjustment of resonator field amplitudes and ion-optical elements by scaling a master tune according the  $m/q$  ratios of the atomic mass and charge state of the ions, in order to conserve an exact velocity profile. The entire accelerator acts then as a high-energy accelerator mass spectrometer; the abundance sensitivity of the accelerator system (before the detection system) was shown<sup>33</sup> to be  $\sim 5 \times 10^{-12}$  for Pb isotopes, separating in the present experiment  $^{146}\text{Sm}$  from  $^{147}\text{Sm}$ . Molecular ions are totally dissociated in the ECR plasma and any molecular ion re-formed at a later stage cannot be injected at the magnetic rigidity corresponding to the high charge-state ions selected for acceleration.

Isobaric separation of  $^{146}\text{Sm}$  and residual  $^{146}\text{Nd}$  ( $((m/q)/\delta(m/q)) \sim 2.4 \times 10^6$ ), beyond the separation power of the accelerator, is achieved in a gas-filled magnetic spectrograph<sup>34</sup>. The ions are then physically separated due to their ( $Z$ -dependent) mean charge state in the gas, are

unambiguously identified and counted by measurement of their position and differential energy loss in a focal-plane detector (fig. 1 right panel).

For a quantitative determination of the atom ratio, the rate of  $^{146}\text{Sm}^{22+}$  ions in the focal-plane detector was normalized to the charge current (of the order of several nA) of the  $^{147}\text{Sm}^{22+}$  beam, transported after proper scaling of the accelerator to an electron-suppressed Faraday cup positioned before the spectrograph entrance. The fraction of ions produced in the ECRIS in the 22+ charge state is considered identical for the two isotopes. The reliability of the  $m/q$  scaling procedure to transport alternatively  $^{146}\text{Sm}^{22+}$  or  $^{147}\text{Sm}^{22+}$  from the ECRIS to the detection setup, was repeatedly checked by measuring the ratio of charge currents for  $^{147}\text{Sm}^{22+}$  and  $^{152}\text{Sm}^{22,23+}$ . The measured  $^{152}\text{Sm}/^{147}\text{Sm}$  ( $1.8\pm0.2$ ), after correcting when necessary for the 23+/22+ population ratio (figs. S1, S2), is consistent with the natural abundance ratio 1.78, showing that the average transmission at different  $m/q$  settings is constant. The uncertainty in the measured abundance, established from repeated measurements, results from fluctuations of this transmission through the complex accelerator system in repeated scaling procedures. The measured atom ratio for each activated sample is shown (fig. 2 and fig. S3), divided by the nominal atom ratio calculated using its alpha activity, its dilution factor (table S1) and the currently adopted half-life values of  $^{146}\text{Sm}$  (103 Ma<sup>3,4</sup>). The double ratio is equivalent to the ratio of our measured half-life to that currently adopted. It is consistently equal to  $0.66\pm0.07$  for the three independent activation reactions and the different dilution ratios and corresponds to a  $^{146}\text{Sm}$  half-life value of  $68\pm7$  Ma ( $1\sigma$ ). For one of the samples the atom ratios were also measured by alternatively counting  $^{146}\text{Sm}^{22+}$  and  $^{147}\text{Sm}^{22+}$  in the focal plane detector, respectively in continuous-wave and attenuated mode. Quantitative attenuation of  $1:10^5$ , required for the abundant  $^{147}\text{Sm}^{22+}$  ions, is obtained with the 12 MHz pulsed and ns-bunched ATLAS beam by chopping ion pulses with an RF sweeper<sup>35</sup> in a (digitally measured) ratio of  $1:10^5$ . The measured atom ratios (fig.2) are

consistent with those described above and confirm that no unaccounted ion losses occur between Faraday cup and the focal plane detector.

## References :

32. Schlapp, M. *et al.*, A new 14 GHz electron-cyclotron-resonance ion source for the heavy ion accelerator facility ATLAS, *Rev. Sci. Inst.* 69, 631-633 (1998)
33. Paul, M. *et al.*, AMS of heavy elements with an ECR ion source and the ATLAS linear accelerator, *Nucl. Inst. Methods Phys. Res. B* 172, 688-692 (2000)
34. Paul, M. *et al.*, Heavy ion separation with a gas-filled magnetic spectrograph, *Nucl. Inst. Methods Phys. Res. A* 277, 418-420 (1989)
35. Paul, M. *et al.*, New AMS Method to Measure the Atom Ratio  $^{146}\text{Sm}/^{147}\text{Sm}$  for a Half-life Determination of  $^{146}\text{Sm}$ , 12th Int. Conf. Accel. Mass Spect., 20-25 Mar, 2011, Wellington, New Zealand.



**Table S1:** Alpha-activity and atom ratios of  $^{146}\text{Sm}$  and  $^{147}\text{Sm}$  in the activated samples measured in this experiment.

Sample notation	$^{147}\text{Sm}$ activity (mBq)	$^{146}\text{Sm}$ activity (mBq)	$^{146}\text{Sm}/^{147}\text{Sm}$ activity ratio ( $10^{-3}$ )	$^{147}\text{Sm}$ activation	Dilution ratio to AMS sample	$^{146}\text{Sm}/^{147}\text{Sm}$ nominal atom ratio <sup>a</sup> ( $10^{-8}$ )	$^{146}\text{Sm}^{22+}/^{147}\text{Sm}^{22+}$ measured atom ratio ( $10^{-8}$ )	$(^{146}\text{Sm}/^{147}\text{Sm})_{\text{meas.}} / (^{146}\text{Sm}/^{147}\text{Sm})_{\text{nominal}}$
G-2	$46.0 \pm 4.7$	$0.185 \pm 0.015$	$4.04 \pm 0.14$	( $\gamma, n$ )	$137 \pm 1$	$2.83 \pm 0.16$	$1.90 \pm 0.21^b$	$0.670 \pm 0.081$
P-3	$9.80 \pm 0.09$	$2.95 \pm 0.05$	$301 \pm 6$	(p, 2n $\epsilon$ )	$551 \pm 8$	$52.7 \pm 2.7$	$31.1 \pm 2.7^b$	$0.590 \pm 0.056$
P-4	$6.28 \pm 0.07$	$2.89 \pm 0.05$	$460 \pm 10$		$894 \pm 10$	$49.6 \pm 2.5$	$30.5 \pm 2.6^c$ $31.5 \pm 1.3^c$ $31.4 \pm 0.9^c$ $31.4 \pm 0.9^c$ $29.6 \pm 0.6^c$ $29.2 \pm 0.6^c$ $29.4 \pm 0.6^c$	$0.615 \pm 0.051$ $0.635 \pm 0.027$ $0.634 \pm 0.018$ $0.633 \pm 0.018$ $0.596 \pm 0.011$ $0.589 \pm 0.012$ $0.593 \pm 0.012$
P-4 ave								$0.61 \pm 0.02$
N-2	$42.3 \pm 10.3$	$0.263 \pm 0.057$	$6.27 \pm 0.14$	(n, 2n)	$102 \pm 0.6$	$5.92 \pm 0.3$	$3.81 \pm 0.35^{b, c}$ $3.26 \pm 0.25^{b, c}$ $3.48 \pm 0.24^{b, c}$	$0.643 \pm 0.064$ $0.551 \pm 0.048$ $0.588 \pm 0.046$
N-2 ave								$0.59 \pm 0.05$
N-7					$33.2 \pm 0.2$	$18.2 \pm 0.9$	$12.0 \pm 0.3^c$ $11.3 \pm 1.0^c$ $13.2 \pm 0.9^c$ $11.6 \pm 0.2^c$	$0.657 \pm 0.031$ $0.622 \pm 0.061$ $0.726 \pm 0.056$ $0.640 \pm 0.027$
N-7 ave								$0.66 \pm 0.05$
N-8					$92.8 \pm 5.0$	$6.51 \pm 0.5$	$4.97 \pm 0.50^c$ $4.37 \pm 0.42^c$ $5.03 \pm 0.30^c$ $4.45 \pm 0.20^c$ $3.54 \pm 0.39^c$ $4.08 \pm 0.45^c$ $4.03 \pm 0.64^c$ $4.10 \pm 0.39^c$ $4.87 \pm 0.09^c$ $4.45 \pm 0.13^c$ $4.94 \pm 0.21^c$ $5.26 \pm 1.18^c$	$0.763 \pm 0.092$ $0.671 \pm 0.078$ $0.772 \pm 0.069$ $0.683 \pm 0.055$ $0.544 \pm 0.070$ $0.627 \pm 0.081$ $0.619 \pm 0.107$ $0.630 \pm 0.073$ $0.748 \pm 0.052$ $0.683 \pm 0.050$ $0.759 \pm 0.060$ $0.808 \pm 0.189$
N-8 ave								$0.69 \pm 0.08$

<sup>a)</sup>  $t_{1/2} (^{146}\text{Sm}) = 103 \pm 5 \text{ Ma}$  <sup>4</sup> and  
 $t_{1/2} (^{147}\text{Sm}) = (1.07 \pm 0.09) \times 10^{11} \text{ a}$  <sup>25</sup>

<sup>b)</sup>  $^{146}\text{Sm}^{22+}/^{152}\text{Sm}^{23+}$  was measured and converted to  $^{146}\text{Sm}/^{147}\text{Sm}$  ratio.

<sup>c)</sup> repeat measurements of the same sample

Figure S1

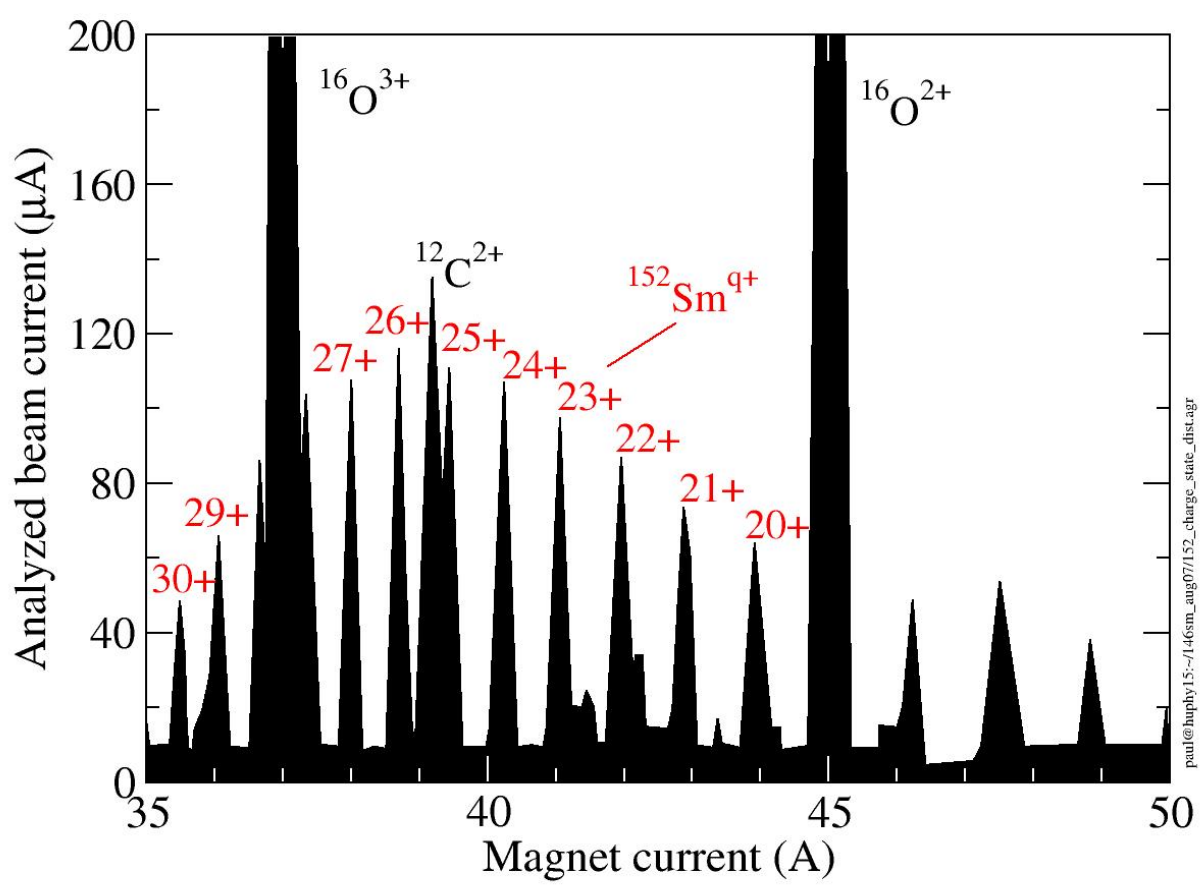


Figure S2

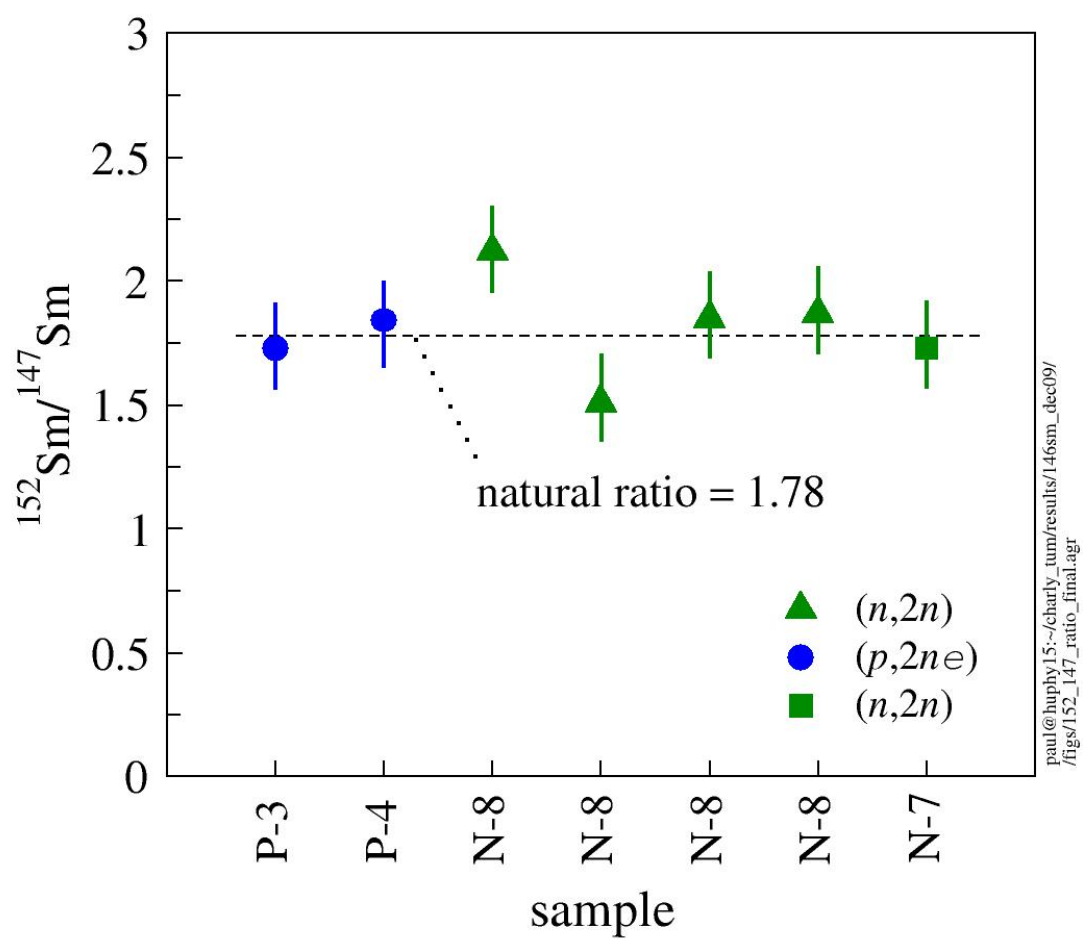


Figure S3

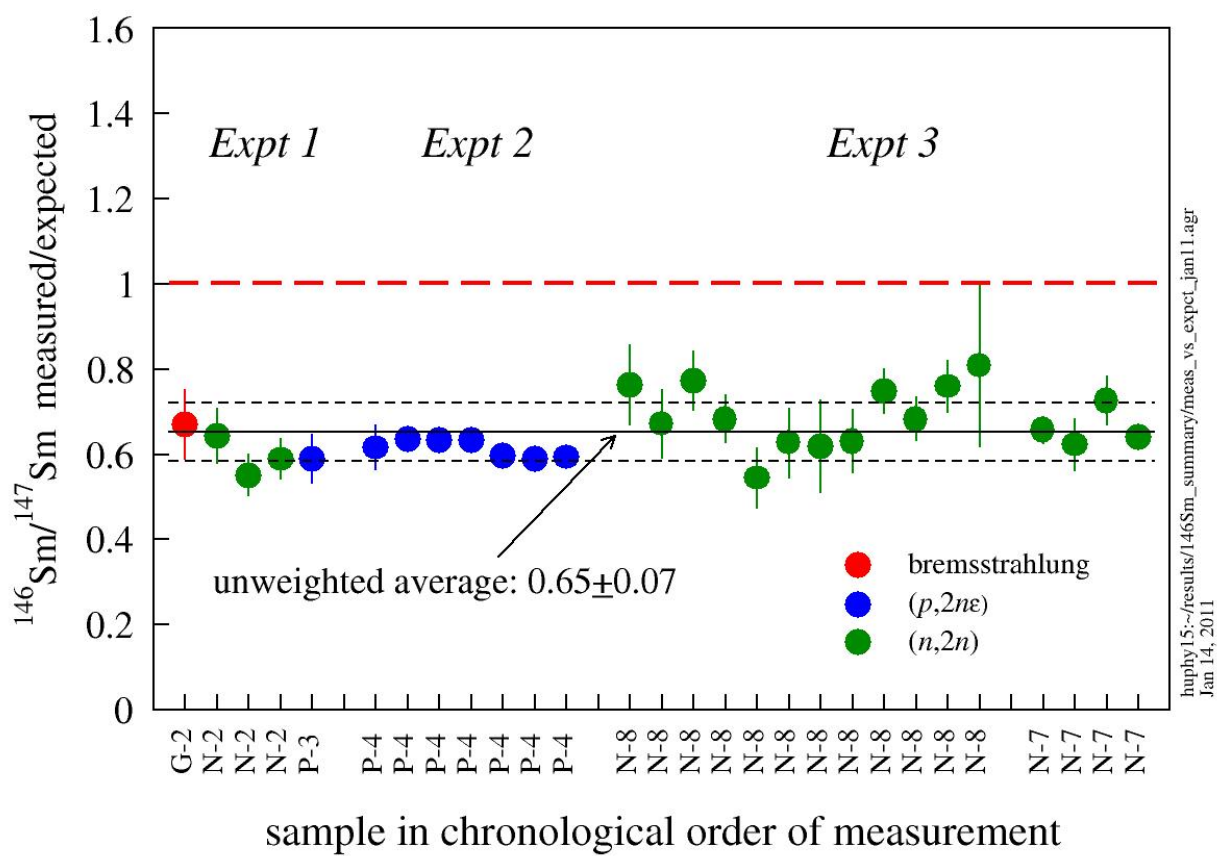


Figure S4a

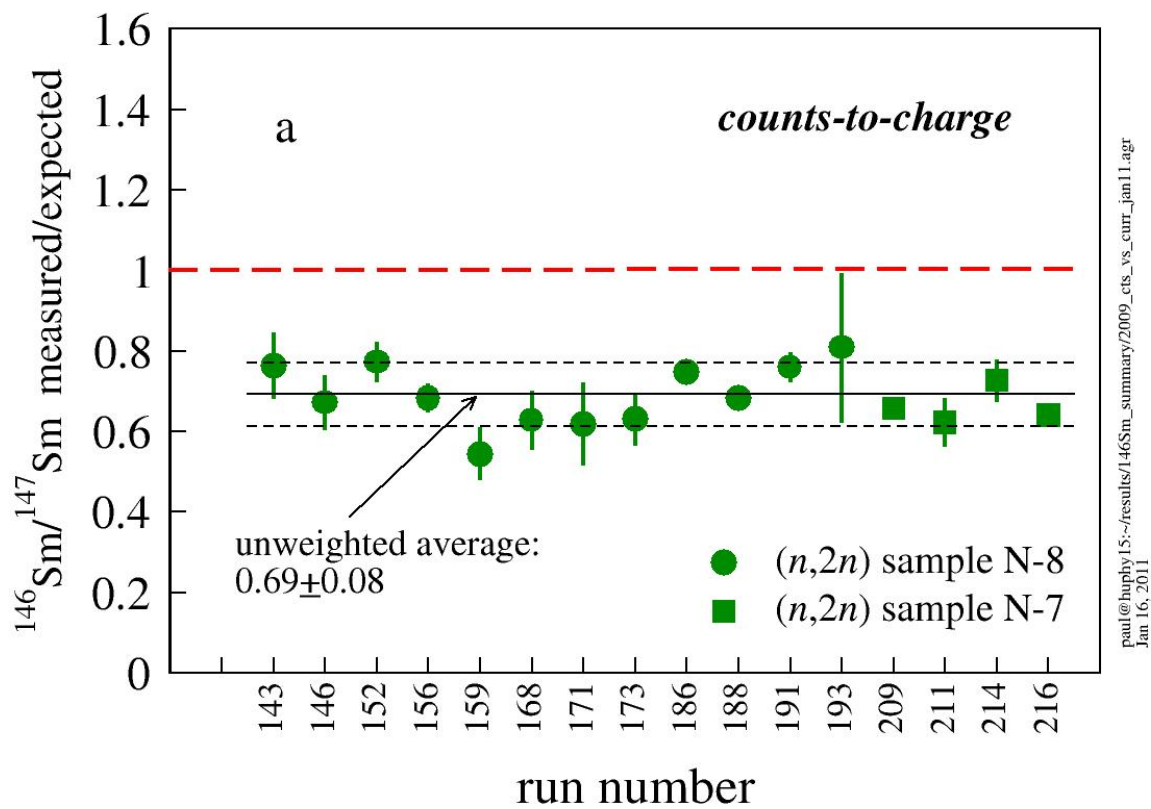


Figure S4b

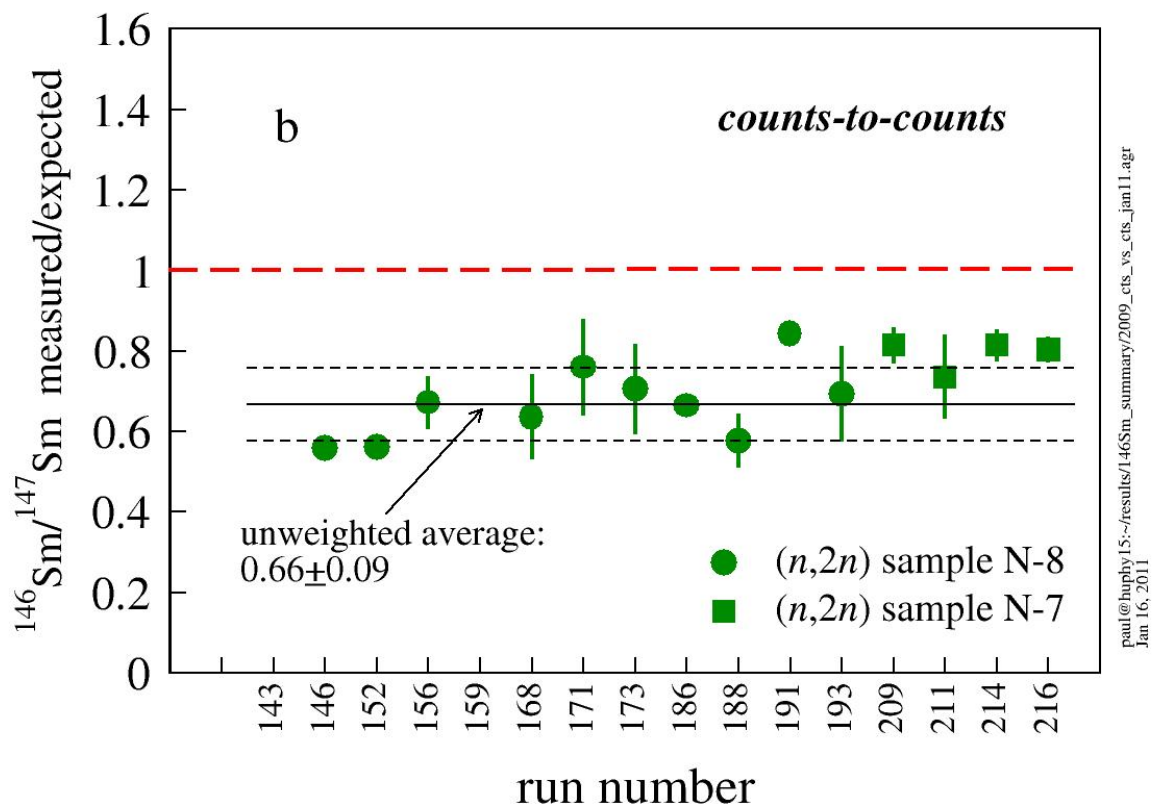


Figure S5

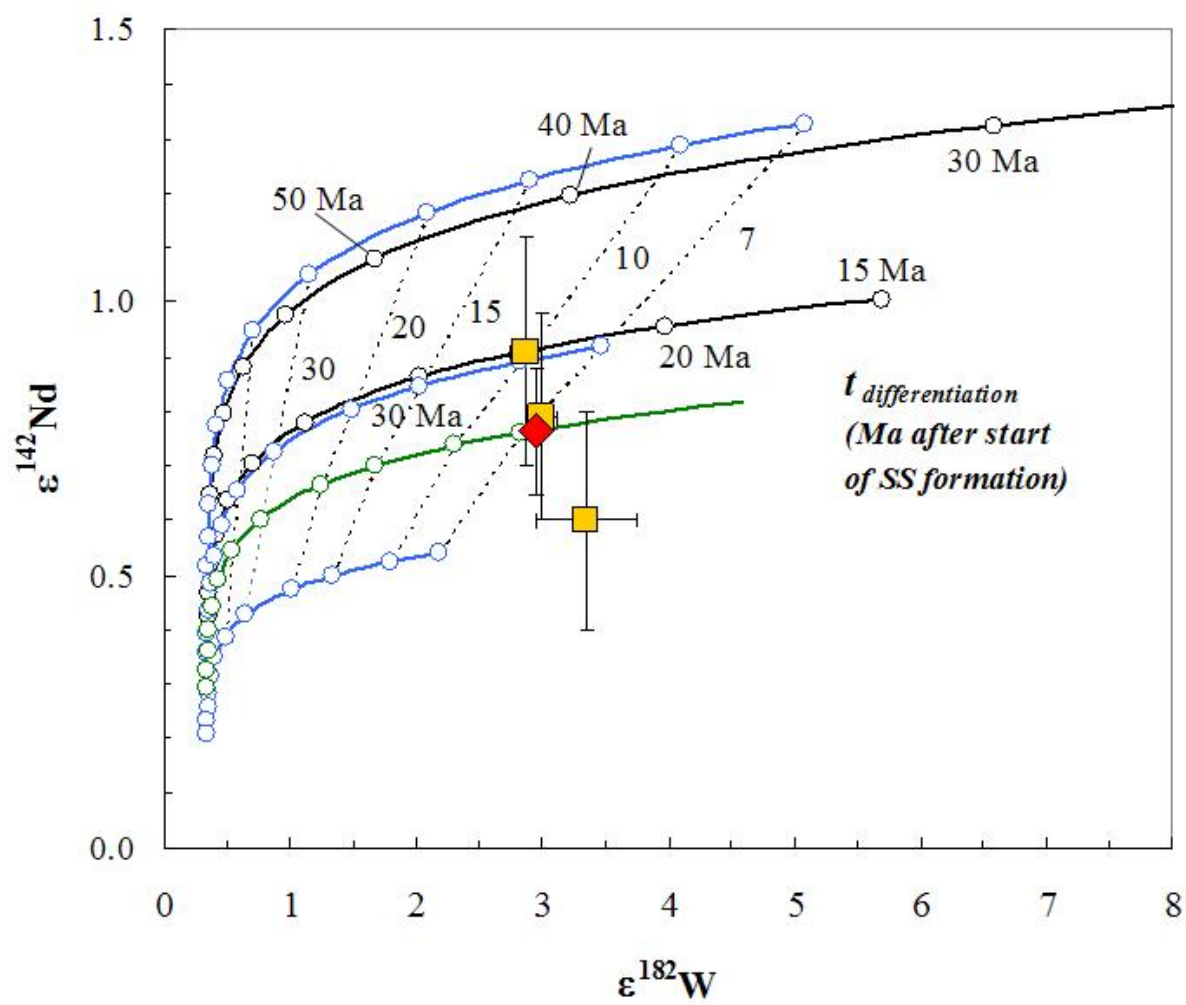


Figure S6

